doi.org/10.1002/cplu.202000497

Diverse Particle Carriers Prepared by Co-Precipitation and Phase Separation: Formation and Applications

Zhu Sun,[a] Baiheng Wu,[a, b] Yixin Ren,[a] Zhongzhen Wang,[a] Chun-Xia Zhao,[c] Mingtan Hai,[d] David A. Weitz,[d] and Dong Chen*[a, b]

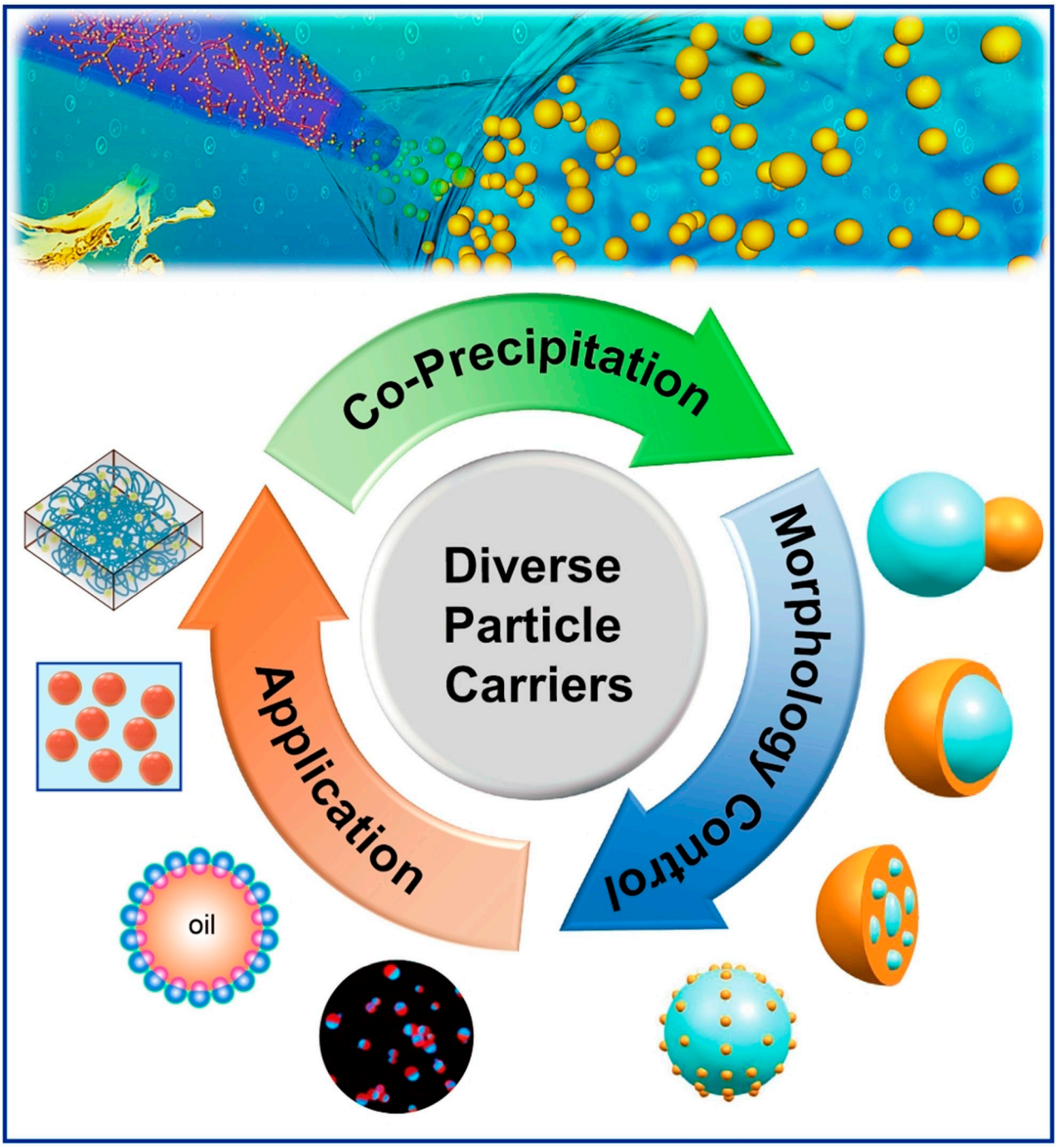

Nanoparticles with diverse structures and unique properties have attracted increasing attention for their widespread applications. Co-precipitation under rapid mixing is an effective method to obtained biocompatible nanoparticles and diverse particle carriers are achieved by controlled phase separation via interfacial tensions. In this Minireview, we summarize the underlying mechanism of co-precipitation and show that rapid mixing is important to ensure co-precipitation. In the binary polymer system, the particles can form four different morphologies, including occluded particle, core-shell capsule, dimer particle, and heteroaggregate, and we demonstrate that the final morphology could be controlled by surface tensions through surfactant, polymer composition, molecular weight, and temperature. The applications of occluded particles, core-shell capsules and dimer particles prepared by co-precipitation or microfluidics upon the regulation of interfacial tensions are discussed in detail, and show great potential in the areas of functional materials, colloidal surfactants, drug delivery, nanomedicine, bio-imaging, displays, and cargo encapsulation.

1. Introduction

Particles can be composed of biocompatible materials, metallic materials, magnetic materials or optical materials,[1–4] and have very rich functionality, showing broad application prospects.[5–15] Nanoprecipitation is a green bottom-up technique to prepare particles through nucleation and growth.[16–18] Generally, the polymer is dissolved in a good solvent, which is then mixed with an anti-solvent. Upon solvent exchange, the polymer precipitates to form particles.[19] To load functional materials inside the particles, co-precipitation is required when both the functional materials and the polymer experience a fast solvent exchange. Flash nanoprecipitation in microfluidic channels or multi inlet vortex mixers has been developed to rapidly mix the good solvent with the anti-solvent to ensure the co-precipitation of polymers.[20] In addition to flash precipitation, sequential precipitation is also an effect way for fast solvent exchange.[21] Compared with other methods, such as emulsion polymerization, nanoprecipitation is a one-step, versatile, scalable and green method to prepare diverse biocompatible nanoparticles with sizes ranging from tens to hundreds of nanometers and readily disperse them in the solution.

In the co-precipitation process of two immiscible polymers, diverse particles with different structural morphologies can be obtained by adjusting the interfacial tensions, including dimer particle, occluded particle, core-shell capsule and heteroaggregate. The type of surfactant, the choice of polymer, the molecular weight of polymer and the mixing temperature all play an important role in determining the final equilibrium particle shape, resulting in a high degree of structural variability of the nanoparticles. The diverse particle carriers allow the customization of cargo loading for targeted applications in functional material, drug delivery, nanomedicine, bio-imaging and display.

The systematic understanding of the particle formation and the precise regulation of their structures could help the design of particles with their properties tailored for specific demands and provide general guidance for the development of novel applications based on the particle carriers.

In this Minireview, we introduce the mechanism of nanoparticle preparation via co-precipitation under rapid mixing, the effect of interfacial tensions on the equilibrium morphology of two immiscible polymers, and the parameters of surfactant, polymer composition, molecular weight and temperature used to tune the particle morphology. At the end, we systematically discuss the applications of particles for functional material, cancer imaging, cargo encapsulation and drug delivery, the applications of core-shell capsules for delivery vehicle, controlled release and functional material, and the applications of dimer particles for colloidal surfactant, display, microlaser and drug release.

2. Mechanism of Co-Precipitation

Nanoprecipitation is a facile green technique to prepare diverse nanoparticles. Polymer molecules precipitate and self-assemble into spherical nanoparticles when the solvent mixes with the anti-solvent. To load the cargo in the nanoparticles, organic active and polymer molecules co-precipitate upon the solvent exchange. During the co-precipitation process, rapid mixing plays an important role in loading the active inside the nanoparticles and achieving nanoparticles with smaller size and size distribution.[25,26,27]

The self-assembly of nanoparticles upon the mixing of solvent and anti-solvent is schematically demonstrated in Figure 1a.[22] Organic active and amphiphilic diblock copolymer are previously dissolved in an organic solvent. When the organic solvent quickly mixes a miscible anti-solvent, both organic active and diblock copolymer precipitate, which involves the nucleation and growth of organic active, τ_{ng}, and the aggregation of copolymer, τ_{agg}. To achieve the co-precipitation of organic active and diblock copolymer and form protected functional nanoparticles, the solvent mixing time, τ_{mix}, should be smaller than the composite process, $\tau_{flash} = \tau_{ng} +$

[a] Z. Sun, B. Wu, Y. Ren, Z. Wang, Prof. D. Chen
Institute of Process Equipment
College of Energy Engineering
Zhejiang University
Zheda Road No. 38, Hangzhou, 310027 (China)
E-mail: chen_dong@zju.edu.cn
[b] B. Wu, Prof. D. Chen
State Key Laboratory of Fluid Power and Mechatronic Systems
Zhejiang University
Zheda Road No. 38, Hangzhou, 310027, China
[c] Prof. C.-X. Zhao
Australian Institute for Bioengineering and Nanotechnology
University of Queensland
St Lucia, QLD 4072 (Australia)
[d] Prof. M. Hai, Prof. D. A. Weitz
John A. Paulson School of Engineering and Applied Sciences
Harvard University
Cambridge, MA 02138 (USA)

τ_{agg}. If τ_{mix} is too large, either the organic active or the diblock copolymer may precipitate well before the other and the two processes may not interact sufficiently with each other to yield active-loaded nanoparticles.

The aggregation of polymers into nanoparticles generally occurs in three stages, involving nucleation of the nanoparticles, growth through aggregation and kinetically locked nanoparticles after a characteristic aggregation time, as shown in Figure 1b. For slow mixing ($\tau_{mix} > \tau_{agg}$), i.e. polymers start to aggregate and form nanoparticles before solvent exchange is complete, both hydrophobic and hydrophilic groups will easily adsorb onto the nanoparticle aggregates, burying the hydrophilic end groups inside the nanoparticles. The particle size will increase over the mixing time, forming large nanoparticles.[23] If solvent exchange completes quickly under rapid mixing ($\tau_{mix} < \tau_{agg}$), polymers aggregate into smaller and more homogeneous nanoparticles with the hydrophilic end groups located at the surface.

Microfluidics, which is capable of precisely controlling the fluids, has demonstrated great potential to ensure rapid mixing of solvent and anti-solvent in microchannels.[24,28,29] We utilized the flow-focusing design of a glass-capillary microfluidic device and enhanced the mixing of ethanol with water via lamellar vortices in the microfluidic channels. Under the rapid solvent exchange, the mixing time ($\tau_{mix} \sim 10$ ms) is shorter than the typical nanoparticle aggregation time ($\tau_{agg} \sim 30$ ms); both curcumin and shellac polymer experience a sudden solvent exchange and co-precipitate to form curcumin-loaded shellac nanoparticles, as shown in Figure 1c.[24] An encapsulation efficiency as high as 98% is thus achieved. If ethanol and water are mixed slowly, shellac would precipitate before curcumin as the water content increases, resulting in failure of active encapsulation.

Another strategy to effectively load active inside the nanoparticles is sequential nanoprecipitation, which form active nanoaggregates first followed by the precipitation of polymer, subsequently encapsulating the active nanoaggregates and forming a core-shell structure, as shown in Figure 1d. Liu et al. first precipitated the drugs into nanoaggregates and then immediately precipitated the polymer to form stable drug-core polymer-shell nanoparticles with a high drug loading capacity up to 58.5% and a high drug encapsulation efficiency up to 98.5%. Various hydrophobic actives could be encapsulated inside the nanoparticles by sequential nanoprecipitation and achieve a high loading capacity and a high encapsulation efficiency. The high-drug-loading nanoparticles also show very high bioavailability, demonstrating an enhanced therapeutic effect and improved safety.[21]

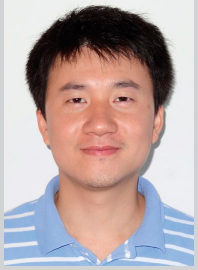

Dong Chen is a professor in the College of Energy Engineering at Zhejiang University (ZJU). Before working at ZJU, he obtained his bachelor's degree from the University of Science and Technology of China, his Ph.D. degree from University of Colorado Boulder, and carried out postdoctoral training at Harvard University. His research mainly focuses on microfluidics, 3D printing and soft matter for applications ranging from functional materials to drug delivery.

3. Morphology Control

During the co-precipitation process, four hierarchical structures could be formed if the polymer system consists of two immiscible polymers, including dimer particle, occluded particle, core-shell capsule and heteroaggregate, as shown in Figure 2a.[34] The final morphology of the binary polymer system is determined by the thermodynamic equilibrium, i.e. the energy minimum state.[35,36] If we define the solvent, phase A, and the two polymers, phase B and phase C, the energy of the binary system is determined by the interfacial tensions between the three phases, i.e. γ_{AB}, γ_{AC} and γ_{BC},[35,37] where γ_{AB}, γ_{AC} and γ_{BC} are the phase A/phase B, phase A/phase C and phase B/phase C interfacial tensions, respectively. A systematic evaluation of the interfacial tensions is generally performed using the spreading coefficients, i.e. $S_A = \gamma_{BC} - (\gamma_{AB} + \gamma_{AC})$, $S_B = \gamma_{AC} - (\gamma_{AB} + \gamma_{BC})$ and $S_C = \gamma_{AB} - (\gamma_{BC} + \gamma_{AC})$.[38] However, the conditions could be simplified that i) $\gamma_{AB} \sim \gamma_{AC} > \gamma_{BC}$ for dimer particle; ii) $\gamma_{AB} > \gamma_{AC} > \gamma_{BC}$ for occluded particle; iii) $\gamma_{AB} > \gamma_{AC} + \gamma_{BC}$ for core-shell capsule; iv) $\gamma_{AB} \sim \gamma_{AC} \sim \gamma_{BC}$ for heteroaggregate. Therefore, the final particle morphology is determined by the interface tensions and could be adjusted to achieve desired structure by controlling the interfacial tensions via surfactant, polymer composition, molecular weight and temperature.

3.1. Effect of Surfactant

At the presence of surfactant molecules, which preferentially adsorb at the interfaces, the polymer/water interfacial tensions could significantly be reduced, causing their surface area to increase. Lee et al. demonstrated that spherical Janus particles of polystyrene (PS) and polyisoprene (PI) or core-shell capsule of amine-terminated PS (PS-NH_2) and PI could change to snowman-like Janus particles in the presence of tween 80, a typical nonionic surfactant soluble in water, as shown in Figure 2b.[30] With tween 80 present in the system, amphiphilic surfactant molecules at the interface interact with both the polymer phase and the aqueous phase, which reduce the polymer/water interfacial tensions, thus resulting in an increase in their surface areas and causing the change to snowman-like Janus particles. Systematic studies have demonstrated that both the type and concentration of surfactants could tune the interfacial tensions to achieve desired particle morphology.[39,40,41]

3.2. Effect of Polymer Composition

Different polymers have different hydrophilicity, which could also affect the polymer/water interfacial tensions; polymer composition is thus another parameter that could tune the

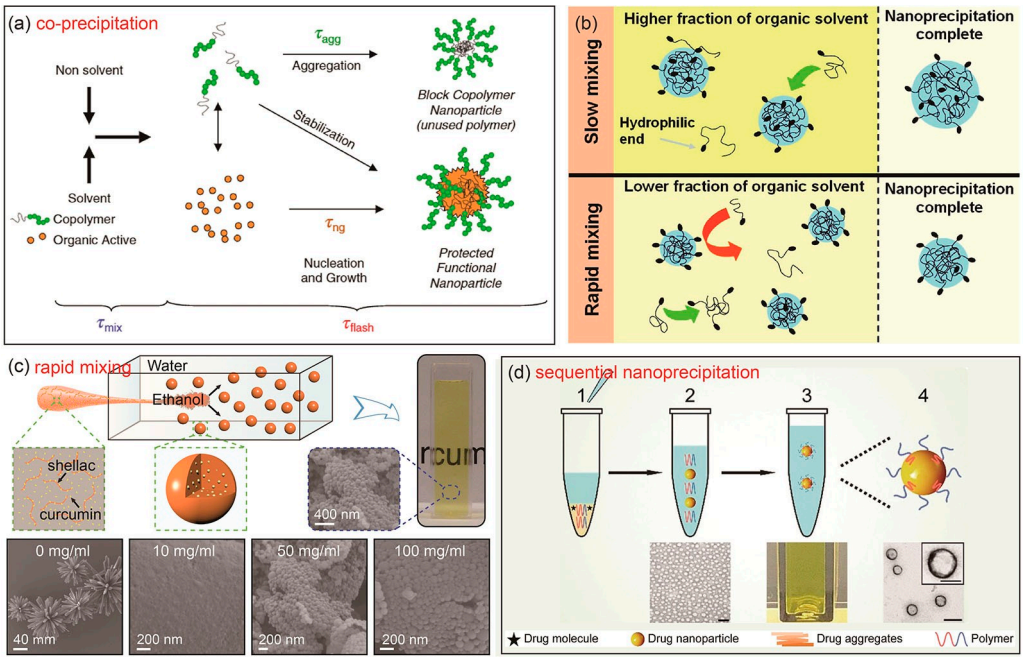

Figure 1. Preparation of nanoparticles by co-precipitation under rapid mixing. (a) Organic active and amphiphilic diblock copolymer co-precipitate to form functional nanoparticles when the solvent mixes with the anti-solvent and the mixing time, τ_{mix}, is smaller than the composite process, τ_{flash}. τ_{flash} is the sum of copolymer aggregation time, τ_{agg}, and active nucleation and growth time, t_{ng}. Reprinted from ref. [22] with permission from CSIRO. (b) Slow mixing ($\tau_{mix} > \tau_{agg}$) results in aggregation of polymers before mixing is complete, burying hydrophilic groups in hydrophobic aggregates. Rapid mixing ($\tau_{mix} < \tau_{agg}$) results in aggregation of polymers after mixing is complete, leading to fewer hydrophilic end groups buried inside the nanoparticles and smaller particle size and size distribution. Reprinted from ref. [23] with permission from American Chemical Society. (c) Co-precipitation of shellac polymer and curcumin is achieved under rapid mixing. Shellac polymer would otherwise precipitate before curcumin under slow mixing, resulting in failure of active encapsulation. Reprinted from ref. [24] with permission from Royal Society of Chemistry. (d) In sequential nanoprecipitation, drugs precipitate first, which are followed by the polymer, covering the drug nanoaggregates and forming a core-shell structure. Reprinted from ref. [21] with permission from Wiley-VCH.

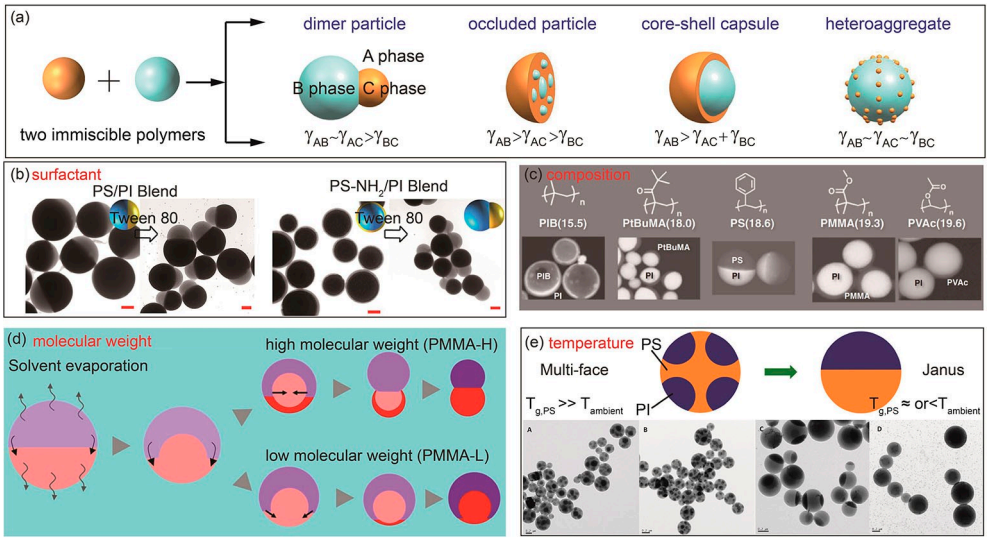

Figure 2. Controlling the particle morphology by interfacial tensions. (a) Four possible morphologies of two immiscible polymers: dimer particle, occluded particle, core-shell capsule and heteroaggregate. The equilibrium particle morphology corresponds to the energy minimum state and is governed by the interfacial tensions. Tuning of the particle morphology by (b) surfactant. Reprinted from ref. [30] with permission from American Chemical Society. (c) polymer composition. Reprinted from ref. [31] with permission. Copyright 2012 Bulletin of the Chemical Society of Japan. (d) molecular weight. Reprinted from ref. [32] with permission from The Chemical Society of Japan. (e) temperature. Reprinted from ref. [33] with permission from the American Chemical Society.

particle morphology, as shown in Figure 2c. Yabu et al. used solubility parameter, δ, to characterize the hydrophilicity of the polymers. Generally, the polymer is more hydrophilic, when the solubility parameter is higher. The experiments show that the combination of PI (δ ~ 16.5) and poly(isobutylene) (PIB, δ ~ 15.5) forms core-shell capsules with relatively hydrophobic PIB core

inside PI shell. In the combination of PI with PtBuMA (δ ~ 18) or PS (δ ~ 18.6), their solubility parameters are relatively close and spherical Janus particles are observed. When the solubility parameter of the polymers is much higher than that of PI, e.g. poly(methyl methacrylate) (PMMA, δ ~ 19.3) or PVAc (δ ~ 19.6), the relatively hydrophilic polymers tend to engulf PI polymer inside the core of the nanoparticles.[31] Generally, when the solubility parameters of the two polymers differ greatly, the system will form a core-shell structure and the polymer with a higher δ will be the shell. When the difference between the solubility parameters is small, a Janus structure is preferred.[42] The experimental results are further confirmed by dissipative particle dynamics simulations.[29]

3.3. Effect of Molecular Weight

Generally, the interfacial tension between polymers increases as the polymer molecular weights increase, leading to morphologic changes.[43,44,45,46] Ge et al. demonstrated that low molecular weight PS (L-PS) and low molecular weight PMMA (L-PMMA) form spherical Janus particles while H-PS and H-PMMA form snowman-like Janus particles.[47] The difference between the final morphologies is attributed to the different interfacial tensions between PS and PMMA with different molecular weights, i.e. the polymer/polymer interfacial tension increases as the polymer molecular weights increase, causing less interfacial area between the polymers. In addition to interfacial tension, Yoshida et al. argued that the effect of molecular weight on the mobility of the polymer also plays an important role in determining the particle morphology. Reducing the molecular weight of PMMA in the dispersed phase accelerates the translational speed of the PMMA-rich phase and enables the engulfing of PBTPA polymer by PMMA polymer, which changes its morphology from an spherical Janus structure to an incomplete core-shell structure, as shown in Figure 2d.[32]

3.4. Effect of Temperature

Temperature could also affect the mobility of polymers and thus the phase separation and the final particle morphology. Sosa et al. co-precipitated glassy polymer (PS) and nonglassy polymer (PI) at temperature below the glass transition temperature (T_g) of PS, below which the vitrified PS polymer inhibits the structural change and the two polymers phase-separate into a nonequilibrium structure of heteroaggregate, as shown in Figure 2e.[33] If the particles are annealed at 135 °C, which is higher than the T_g of PS, PS aggregates start to form a single domain, forming spherical Janus particles. This is because vitrified PS aggregates are able to anneal above T_g to reach the thermal equilibrium state. At even higher temperature, the PS bulb could even detach from the PI bulb. By using thermoresponsive poly(N-isopropylacrylamide) (pNIPAM), which becomes hydrophobic above its low critical solution temperature (LCST), Motoyoshi et al. demonstrated reversible changes between core-shell capsules (T LCST) and Janus particles (T LCST) of the binary system of PNIPAM and poly(N-isopropylacrylamide-co-N-dodecylacrylamide) (TRP) by changing the temperature.[42]

In general, the addition of surfactants could significantly reduce the polymer/water interfacial tensions, causing their surface area to increase; hydrophilic polymers tend to increase the polymer/water surface area while hydrophobic polymers tend to minimize the polymer/water surface area; the interfacial tension between polymers increases as the polymer molecular weights increase, leading to the decrease of the polymer/polymer surface area; particles could kinetically be locked in a high-energy intermediate state at low temperature, which could anneal to the equilibrium state at high temperature. These rules will provide guidance for the design and fabrication of functional nanoparticle with desired structures.

4. Applications

4.1. Applications of Nanoparticles

As discussed above, nanoparticles with a high degree of structural variability could be achieved by co-precipitation and controlled phase separation. Among the four morphologies, occluded nanoparticles are widely used as a versatile vehicle to load various functional materials, showing a high degree of functional variability; diverse nanoparticles are developed for functional material, cancer imaging, cargo encapsulation and drug delivery, as shown in Figure 3.

By loading chlorophyll in shellac polymer via co-precipitation and subsequently incorporating chlorophyll-loaded shellac nanoparticles into calcite crystals grown in the gel medium, we developed an organic-inorganic hybrid functional material for bioactive molecules, as shown in Figure 3a.[48] The hybrid material could greatly improve the shelf-life of chlorophyll and possess a unique pH-triggered release, mimicking the pH changes in human stomach and intestine.

When nanoparticles are loaded with fluorescent dyes, they could be used for sensing and imaging in living cells with very high spatial and temporal resolution. Runser et al. monitored the behavior of Rhodamine B-loaded nanoparticles at the level of single particle and showed that the particles diffuse freely within the cytoplasm of living cells.[52] Fathi et al. prepared biliverdin-loaded nanoparticles, a naturally occurring heme-based pigment, and demonstrated that injection of the nanoparticles into mice can lead to enhanced photoacoustic signals.[53] Li et al. prepared charge-conversion nanoparticles with amphiphilic polymers at the surface by flash nanoprecipitation. The critical pH for the charge transition (pH ~ 7.2) enables negative charge at physiological pH, resisting protein adsorption, and the negative-to-positive charge transition occurs under slightly acidic condition, increasing their cellular uptake at weakly acidic tumor tissue, as shown in Figure 3b.[49]

The nanoparticles formed by co-precipitation are widely used to encapsulate cargos, such as β-carotene, doxorubicin, paclitaxel, curcumin, insulin, DNA and so on, to solve the problems of low water solubility, poor stability, poor bioavailability and controlled release.[54,55,56,57,58,59,60,61,62,63] Lu et al. used

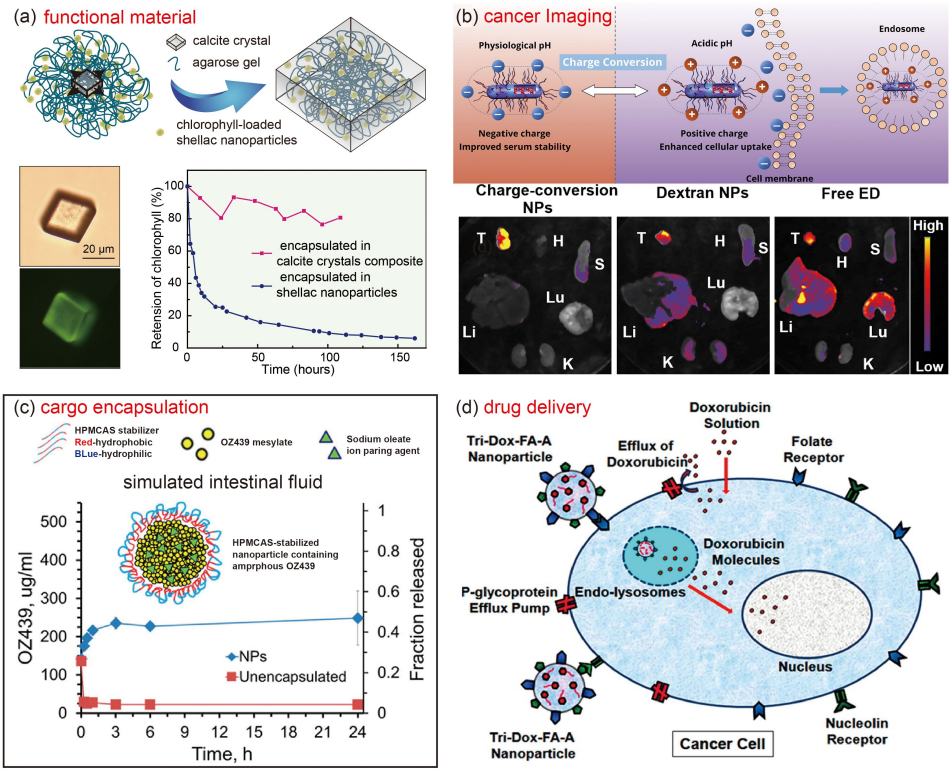

Figure 3. Applications of nanoparticles. Diverse designs of nanoparticles for (a) functional material, e.g. chlorophyll-loaded shellac nanoparticles in gel-grown calcite crystals. Reprinted from ref. [48] with permission from Elsevier. (b) cancer imaging, e.g. charge-tunable nanoparticles for improved serum stability and enhanced cancer cellular uptake. Reprinted from ref. [49] with permission from the American Chemical Society. (c) cargo encapsulation, e.g. increased bioavailability of mesylate-loaded nanoparticles in simulated intestinal fluid. Reprinted from ref. [50] with permission from the American Chemical Society. (d) drug delivery, e.g. dual-targeted (AS1411 aptamer and folic acid) and pH-sensitive pPEGMA-PCL-pPEGMA nanoparticles for targeted doxorubicin delivery in cancer therapy. Reprinted from ref. [51] with permission from the American Chemical Society.

flash nanoprecipitation to prepare water-dispersible nanoparticles of 50–400 nm in size containing OZ439, a poor orally bioavailable but promising candidate for single-dose malaria treatment. Compared with unencapsulated drug, OZ439-loaded nanoparticles show characteristics of sustained release and the released drug concentration is several times higher, effectively improving the drug's bioavailability, as shown in Figure 3c.[50] The nanoparticles could also reduce the amount of drug required per patient and the cost for the development of single-dose oral malaria therapeutics.

By engineering the polymers, nanoparticles can also achieve target drug delivery by actively delivering the particles to the diseased tissues through enhanced permeability and retention (EPR) effect.[64,65,66] Lale et al. prepared AS1411 aptamer and folic acid functionalized pH-responsive pPEGMA-PCL-pPEGMA polymeric nanoparticles via atom transfer radical polymerization (ATRP). The folate-mediated endocytosis improves the targeting efficiency of the nanoparticles to the cancer cells and their accumulation. Doxorubicin is then released under the acidic environment of cancer cells via the breakage of acid-labile hydrazone linkage, through which doxorubicin is conjugated to the triblock polymer, as shown in Figure 3d.[51] Gao et al. prepared DM1-NO, a nitrosylated maytansine analogue, and encapsulated it inside PLGA-b-PEG nanoparticles. The toxicity of DM1 is suppressed by nitrosylation and encapsulation. Under irradiation at the tumor site, oxidative stress increases, leading to the S–N bond breakage and the release of DM1 and NO, both of which could suppress the tumors.[67]

4.2. Applications of Core-Shell Capsules

Similar to occluded particles, capsules with a hierarchical core-shell structure are widely used for delivery vehicle, controlled release and functional material, as shown in Figure 4.[70,71,72,73,74,75] Via one-step co-precipitation and controlled phase separation, we actively encapsulated various oils in the biocompatible core-shell nanocapsules and used them as delivery vehicle to improve the bioavailability of capsanthin, paclitaxel and doxorubicin, as shown in Figure 4a.

In addition to co-precipitation, microfluidics has also been applied to prepare uniform core-shell microcapsules via controlled phase separation.[76,77,78] The preparation of microcapsules by microfluidics generally use single emulsions as templates or double emulsions as templates. When using single emulsions as templates, the microcapsules are prepared by the controlled phase separation of the polymer upon solvent evaporation.[79,80] Tang et al. used a flow-focusing microfluidics device and prepared uniform droplets of oil and polymer in chloroform. Upon fast solvent evaporation, the polymer phase

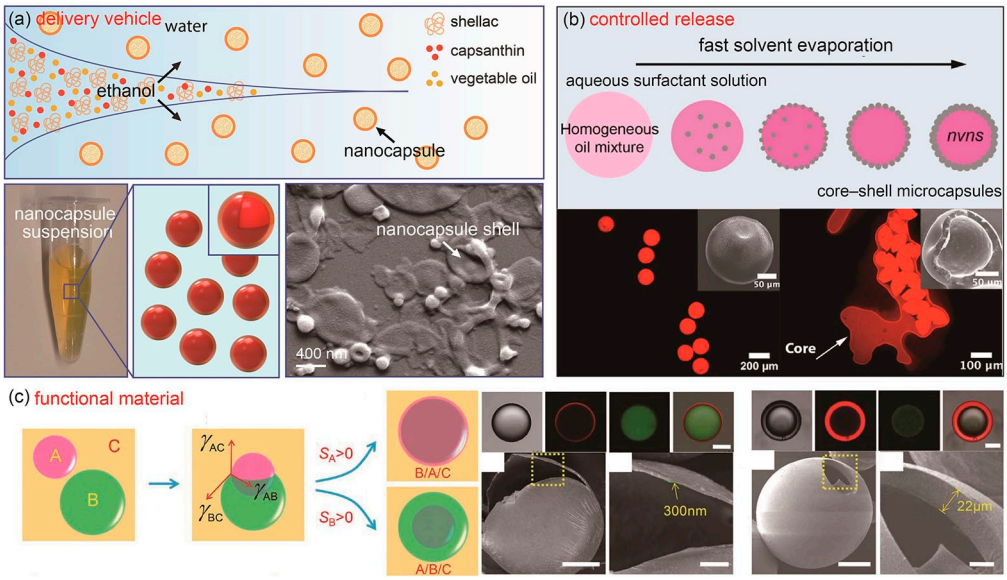

Figure 4. Applications of core-shell capsules. (a) Controlled preparation of hierarchical core-shell nanocapsules by co-precipitation upon rapid mixing and their application as delivery vehicle. (b) Core-shell microcapsules formed by the precipitation of cPPA polymer at the water/oil interface upon fast solvent evaporation and their controlled release of the core material by crushing. Reprinted from ref. [68] with permission from the American Chemical Society. (c) Thickness-tunable microcapsules prepared by wetting of one liquid by the other and their application as functional material. Reprinted from ref. [69] with permission from the Royal Society of Chemistry.

separates into small polymer-rich droplets, which then migrate to the water/oil interface, coalescing to form core-shell microcapsules, as shown in Figure 4b.[68] The oil could subsequently be released by dissolving the polymer shells under acidic environment.

When using double emulsions as templates, the interfacial tensions between the phases are engineered. Deng et al. adjusted the spreading coefficients between the phases so that droplets of one fluid completely engulf droplets of the other immiscible fluid, as shown in Figure 4c.[69] These core-shell microcapsules could be used as templates to develop various functional materials.

4.3. Applications of Dimer Particles

Dimer particles with two different chemical compositions, also called Janus particles, have great potential in colloidal surfactant, display, microlaser and drug release.[85,86,87,88,89] Similar to surfactant molecules, Janus dimer particles could also be amphiphilic and have a much stronger anchoring strength at the water/oil interface. We successfully prepared amphiphilic dimer particles consisting of a hydrophobic PLA bulb and a hydrophilic shellac-PEG bulb and demonstrated that by engineering the diameter ratio of the dimer particles, i.e. the ratio of the hydrophobic bulb to the hydrophilic bulb, the curvature of the water/oil interface could easily be tuned, thus giving a flexible control over the type of emulsions, as shown in Figure 5a.[81] By designing the Janus particles, shape-changeable and amphiphilicity-tunable colloidal surfactants are also developed, which could reverse the emulsion type under proper conditions, such as pH changes.[90,91,92]

A well-known application of Janus dimer particles with asymmetric optical and magnetic properties is display. The motion of two-color Janus particles can be controlled remotely under the action of external electric or magnetic field. By magnetizing the Janus particles consisting of PS bulb and Fe_3O_4 bulb along different direction, two kinds of magnetic Janus particles (J-1 magnetized along the PS/Fe_3O_4 interface and J-2 magnetized perpendicular to the PS/Fe_3O_4 interface) are achieved and their applications as switch and display are demonstrated in Figure 5b.[82] The magnetic Janus particles can easily be flipped or rotated under an external magnetic field, making it a good pixel unit in display,[93,94] and a magnetic needle can be used to freely write on the display panel.[95]

Encapsulation of functional materials in the dimer particles enables the functionalization of the particles for microlaser and imaging. Wei et al. took advantages of the different affinity of different dyes with different polymers and successfully prepared dual-color fluorescent dimer particles, whose two sides are distinctively doped with hydrophilic and hydrophobic dyes for the achievement of dual-color microlaser, as shown in Figure 5c.[83] When loaded with iron oxides, the dimer nanoparticles could be applied to sensitive MPI tracking after implantation into mice.[96]

Janus dimer particles could also be used as carriers to load different drugs simultaneously for drug delivery and nanomedicine.[97,98,99] Li et al. made oil-in-water single emulsions using microfluidics and obtained biocompatible and biodegradable PLGA/PCL Janus dimer particles by precisely controlling the phase separation of the two immiscible components upon solvent evaporation. Because PLGA is hydrophilic and PCL is hydrophobic, different drugs with different hydrophobicity can simultaneously be encapsulated in different bulbs. For example,

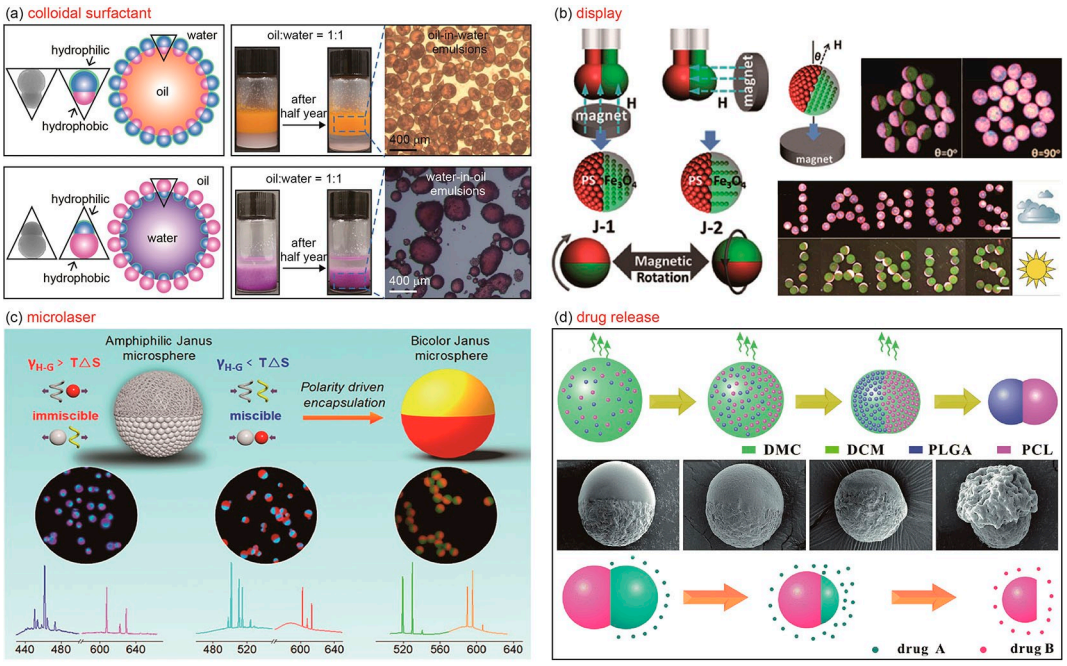

Figure 5. Application of dimer particles. (a) Application of amphiphilic dimer particles as colloidal surfactants and tuning of the interfacial curvature and thus the emulsion type by the particle diameter ratio. Reprinted from ref. [81] with permission from Wiley-VCH. (b) Preparation of magnetic dimer particles by microfluidics and their application as display. Reprinted from ref. [82] with permission from the Royal Society of Chemistry. (c) Bicolor Janus particles prepared by polarity-driven encapsulation of two different dyes in separate bulbs and their application as microlaser. Reprinted from ref. [83] with permission from the American Chemical Society. (d) Preparation of PLGA/PCL Janus particles by solvent evaporation and phase separation and their application for drug release. Reprinted from ref. [84] with permission from the Royal Society of Chemistry.

the hydrophilic fluorescent dye, Rhodamine B, preferentially stains PLGA bulb instead of PCL bulb. In addition, the degradation rate of PLGA is much faster than that of PCL and Janus dimer particles thus can realize controllable and programmable drug release, first releasing drug A in PLGA and then releasing drug B in PCL, as shown in Figure 5d.[84] Two drugs simultaneously loaded in Janus dimer particles could also show pH-sensitive release of individual drugs.[100] Local inhalation treatment of mice bearing lung tumors using Janus dimer nanoparticles loaded with two anticancer drugs are able to successfully suppress the tumor growth.[101]

5. Conclusions and Outlook

Co-precipitation under rapid mixing and controlled phase separation by tuning the interfacial tensions are a versatile method to prepare occluded particle, core-shell capsule, dimer particle and heteroaggregate, providing countless interesting possibilities in various fields. The diverse particle carries provide an excellent platform for the development of various functional materials on demand. For example, by loading drugs, dyes or magnets, the particles could be applied in drug delivery, imaging or display, respectively. The systematic understanding of the particle formation and the precise regulation of their structures will help the design of particles with their properties optimized for targeted applications and provide general guidance for the development of novel applications based on the particle carriers. We believe that the diverse particle carriers will play a more and more important role in both science and technology, especially their applications in biological fields.

Acknowledgements

This work is supported by the National Natural Science Foundation of China (Grant No. 21878258 and 11704331), Zhejiang Provincial Natural Science Foundation of China (Grant No. Y20B060027) and Zhejiang University Education Foundation Global Partnership Fund. This work is also supported by the National Science Foundation (DMR1310266) and the Harvard Materials Research Science and Engineering Center (DMR-1420570). B. Wu acknowledges the financial support from China postdoctoral Science Foundation (Grant No. 2019TQ0274). C.-X. Zhao acknowledges the financial support from the Australian Research Council under Future Fellowship (FT140100726).

Conflict of Interest

The authors declare no conflict of interest.

Keywords: cargo delivery · interfacial tension · microfluidics · nanostructures · precipitation

[1] T. Y. Tu, W. J. Zhou, M. W. Wang, X. H. Guo, L. Li, M. A. C. Stuart, J. Y. Wang, *Ind. Eng. Chem. Res.* **2020**, *59*, 11080–11086.
[2] X. Wang, J. Sheng, M. Yang, *Chinetsu* **2019**, *30*, 533–540.
[3] K. Peng, F. T. Lv, H. Lu, J. W. Wang, H. Zhao, L. B. Liu, S. Wang, *Chinetsu* **2020**, *31*, 755–758.
[4] V. Oleksa, H. Mackova, V. Patsula, A. Dydowiczova, O. Janouskova, D. Horak, *ChemPlusChem* **2020**, *85*, 1156–1163.
[5] O. Shapoval, O. Kaman, J. Hromádková, D. Vavřík, D. Jirák, D. Machová, J. Parnica, D. Horák, *ChemPlusChem* **2019**, *84*, 1135–1139.
[6] Y. Liu, G. Yang, D. Zou, Y. Hui, K. Nigam, A. P. Middelberg, C.-X. Zhao, *Ind. Eng. Chem. Res.* **2019**, *59*, 4134–4149.
[7] L. Zhang, Q. Chen, Y. Ma, J. Sun, *ACS Applied Bio Materials* **2019**, *3*, 107–120.
[8] B. Guo, E. Middha, B. Liu, *ACS Nano* **2019**, *13*, 2675–2680.
[9] Z. Chen, C. Wu, Z. F. Zhang, W. P. Wu, X. F. Wang, Z. Q. Yu, *Chinetsu* **2018**, *29*, 1601–1608.
[10] S. Zhao, R. R. Tian, B. Q. Shao, Y. Feng, S. W. Yuan, L. P. Dong, L. Zhang, K. Liu, Z. X. Wang, H. P. You, *ACS Appl. Mater. Interfaces* **2019**, *11*, 394–402.
[11] Q. S. Lin, Z. H. Li, Q. Yuan, *Chinetsu* **2019**, *30*, 1547–1556.
[12] W. Q. Yu, M. Shevtsov, X. C. Chen, H. L. Gao, *Chinetsu* **2020**, *31*, 1366–1374.
[13] J. C. Bulanadi, A. Q. Xue, X. J. Gong, P. A. Bean, S. M. Julovi, L. de Campo, R. C. Smith, M. J. Moghaddam, *ChemPlusChem* **2020**, *85*, 1283–1291.
[14] Y. Liu, Y. Hui, R. Ran, G. Z. Yang, D. Wibowo, H. F. Wang, A. P. Middelberg, C. X. Zhao, *Adv. Healthcare Mater.* **2018**, *7*, 1800106.
[15] J. Li, B. Li, J. Sun, C. Ma, S. Wan, Y. Li, R. Göstl, A. Herrmann, K. Liu, H. Zhang, *Adv. Mater.* **2020**, *32*, 2000964.
[16] H. Fessi, F. Puisieux, J. P. Devissaguet, N. Ammoury, S. Benita, *Int. J. Pharm.* **1989**, *55*, R1–R4.
[17] S. Guterres, H. Fessi, G. Barratt, J.-P. Devissaguet, F. Puisieux, *Int. J. Pharm.* **1995**, *113*, 57–63.
[18] D. F. Liu, H. B. Zhang, S. Cito, J. Fan, E. Makila, J. Salonen, J. Hirvonen, T. M. Sikanen, D. A. Weitz, H. A. Santos, *Nano Lett.* **2017**, *17*, 606–614.
[19] C. G. Barreras-Urbina, B. Ramirez-Wong, G. A. Lopez-Ahumada, S. E. Burruel-Ibarra, O. Martinez-Cruz, J. A. Tapia-Hernandez, F. R. Felix, *Int. J. Food Prop.* **2016**, *19*, 1912–1923.
[20] S. Bobbala, S. D. Allen, E. A. Scott, *Nanoscale* **2018**, *10*, 5078–5088.
[21] Y. Liu, G. Yang, T. Baby, D. Chen, D. A. Weitz, C. X. Zhao, *Angew. Chem. Int. Ed.* **2020**, *59*, 4720–4728.
[22] B. K. Johnson, R. K. Prud'homme, *Aust. J. Chem.* **2003**, *56*, 1021–1024.
[23] R. Karnik, F. Gu, P. Basto, C. Cannizzaro, L. Dean, W. Kyei-Manu, R. Langer, O. C. Farokhzad, *Nano Lett.* **2008**, *8*, 2906–2912.
[24] L. L. Kong, R. Chen, X. Z. Wang, C. X. Zhao, Q. S. Chen, M. T. Hai, D. Chen, Z. Z. Yang, D. A. Weitz, *Lab Chip* **2019**, *19*, 2089–2095.
[25] Y. Liu, G. Z. Yang, D. Zou, Y. Hui, K. Nigam, A. P. J. Middelberg, C. X. Zhao, *Ind. Eng. Chem. Res.* **2020**, *59*, 4134–4149.
[26] T. I. Morozova, V. E. Lee, N. Bizmark, S. S. Datta, R. K. Prud'homme, A. Nikoubashman, R. D. Priestley, *ACS Cent. Sci.* **2020**, *6*, 166–173.
[27] W. S. Saad, R. K. Prud'homme, *Nano Today* **2016**, *11*, 212–227.
[28] A. Nikoubashman, V. E. Lee, C. Sosa, R. K. Prud'homme, R. D. Priestley, A. Z. Panagiotopoulos, *ACS Nano* **2016**, *10*, 1425–1433.
[29] Y. Liu, C. Y. Cheng, Y. Liu, R. K. Prud'homme, R. O. Fox, *Chem. Eng. Sci.* **2008**, *63*, 2829–2842.
[30] V. E. Lee, C. Sosa, R. Liu, R. K. Prud'homme, R. D. Priestley, *Langmuir* **2017**, *33*, 3444–3449.
[31] H. Yabu, *Bull. Chem. Soc. Jpn.* **2012**, *85*, 265–274.
[32] S. Yoshida, S. Kikuchi, S. Kanehashi, K. Okamoto, K. Ogino, *Materials* **2018**, *11*, 582.
[33] C. Sosa, V. E. Lee, L. S. Grundy, M. J. Burroughs, R. Liu, R. K. Prud'homme, R. D. Priestley, *Langmuir* **2017**, *33*, 5835–5842.
[34] A. Loxley, B. Vincent, *J. Colloid Interface Sci.* **1998**, *208*, 49–62.
[35] D. C. Sundberg, Y. G. Durant, *Polym. React. Eng.* **2003**, *11*, 379–432.
[36] X. D. Cao, W. X. Li, T. Ma, H. Dong, *RSC Adv.* **2015**, *5*, 79969–79975.
[37] L. Girifalco, R. J. Good, *J. Phys. Chem.* **1957**, *61*, 904–909.
[38] S. Torza, S. Mason, *J. Colloid Interface Sci.* **1970**, *33*, 67–83.
[39] N. Saito, Y. Kagari, M. Okubo, *Langmuir* **2006**, *22*, 9397–9402.
[40] N. Saito, Y. Kagari, M. Okubo, *Langmuir* **2007**, *23*, 5914–5919.
[41] Y. Wang, B. H. Guo, X. Wan, J. Xu, X. Wang, Y. P. Zhang, *Polymer* **2009**, *50*, 3361–3369.
[42] K. Motoyoshi, A. Tajima, T. Higuchi, H. Yabu, M. Shimomura, *Soft Matter* **2010**, *6*, 1253–1257.
[43] D. Broseta, L. Leibler, L. O. Kaddour, C. Strazielle, *J. Chem. Phys.* **1987**, *87*, 7248–7256.
[44] Y. C. Chen, V. Dimonie, M. S. Elaasser, *J. Appl. Polym. Sci.* **1992**, *46*, 691–706.
[45] T. Tanaka, R. Nakatsuru, Y. Kagari, N. Saito, M. Okubo, *Langmuir* **2008**, *24*, 12267–12271.
[46] H. Taherzadeh, K. Ogino, *Open* **2015**, *5*, 37.
[47] X. P. Ge, M. Z. Wang, X. Ji, X. W. Ge, H. R. Liu, *Colloid Polym. Sci.* **2009**, *287*, 819–827.
[48] L. L. Kong, X. Y. Jin, D. P. Hu, L. Y. Feng, D. Chen, H. Y. Li, *Chinetsu* **2019**, *30*, 2351–2354.
[49] M. Li, Y. S. Xu, J. L. Sun, M. W. Wang, D. H. Yang, X. H. Guo, H. Y. Song, S. Cao, Y. F. Yan, *ACS Appl. Mater. Interfaces* **2018**, *10*, 10752–10760.
[50] H. D. Lu, K. D. Ristroph, E. L. K. Dobrijeyic, J. Feng, S. A. McManus, Y. Y. Zhang, W. D. Mulhearn, H. Ramachandruni, A. Patel, R. K. Prud'homme, *ACS Infect. Dis.* **2018**, *4*, 970–979.
[51] S. V. Lale, R. G. Aswathy, A. Aravind, D. S. Kumar, V. Koul, *Biomacromolecules* **2014**, *15*, 1737–1752.
[52] A. Runser, D. Dujardin, P. Ernst, A. S. Klymchenko, A. Reisch, *ACS Appl. Mater. Interfaces* **2020**, *12*, 117–125.
[53] P. Fathi, H. J. Knox, D. Sar, I. Tripathi, F. Ostadhossein, S. K. Misra, M. B. Esch, J. Chan, D. Pan, *ACS Nano* **2019**, *13*, 7690–7704.
[54] M. H. M. Leung, A. Q. Shen, *Langmuir* **2018**, *34*, 3961–3970.
[55] W. Badri, A. El Asbahani, K. Miladi, A. Baraket, G. Agusti, Q. A. Nazari, A. Errachid, H. Fessi, A. Elaissari, *J. Drug Delivery Sci. Technol.* **2018**, *46*, 234–242.
[56] J. Far, M. Abdel-Haq, M. Gruber, A. Abu Ammar, *ACS Omega* **2020**, *5*, 7432–7439.
[57] K. Chen, Z. Fu, M. Wang, Y. Lv, C. Wang, Y. Shen, Y. Wang, H. Cui, X. Guo, *J. Agric. Food Chem.* **2018**, *66*, 8246–8252.
[58] D. Massella, E. Celasco, F. Salaün, A. Ferri, A. A. Barresi, *Polymer* **2018**, *10*, 1092.
[59] R. Lancheros, C. A. Guerrero, R. D. Godoy-Silva, *J. Nanotechnol.* **2018**, *2018*, 3620373.3620371–3620373.3620311.
[60] R. Ghaffari, N. Eslahi, E. Tamjid, A. Simchi, *ACS Appl. Mater. Interfaces* **2018**, *10*, 19336–19346.
[61] M. Galliani, G. Signore, *ChemPlusChem* **2019**, *84*, 1653–1658.
[62] G. Z. Yang, Y. Liu, H. F. Wang, R. Wilson, Y. Hui, L. Yu, D. Wibowo, C. Zhang, A. K. Whittaker, A. P. J. Middelberg, C. X. Zhao, *Angew. Chem. Int. Ed.* **2019**, *58*, 14357–14364.
[63] G. Z. Yang, Y. Liu, S. Jin, C. X. Zhao, *ChemBioChem* **2020**.
[64] S. Dufort, L. Sancey, J. L. Coll, *Adv. Drug Delivery Rev.* **2012**, *64*, 179–189.
[65] H. Maeda, *J. Controlled Release* **2012**, *164*, 138–144.
[66] M. He, L. Yu, Y. Yang, B. Zou, W. Ma, M. Yu, J. Lu, G. Xiong, Z. Yu, A. Li, *Chinetsu* **2020**, DOI:10.1016/j.cclet.2020.05.034.
[67] S. Gao, W. Z. Zhang, R. J. Wang, S. P. Hopkins, J. C. Spagnoli, M. Racin, L. Bai, L. Li, W. Jiang, X. Y. Yang, C. Lee, K. Nagata, E. W. Howerth, H. Handa, J. Xie, Q. J. Ma, A. Kumar, *ACS Nano* **2020**, *14*, 1468–1481.
[68] S. Tang, M. Yourdkhani, C. M. Possanza Casey, N. R. Sottos, S. R. White, J. S. Moore, *ACS Appl. Mater. Interfaces* **2017**, *9*, 20115–20123.
[69] N.-N. Deng, W. Wang, X.-J. Ju, R. Xie, D. A. Weitz, L.-Y. Chu, *Lab Chip* **2013**, *13*, 4047–4052.
[70] D. Wibowo, Y. Hui, A. P. J. Middelberg, C. X. Zhao, *Adv. Colloid Interface Sci.* **2016**, *236*, 83–100.
[71] M. A. Trojer, A. A. Gabul-Zada, A. Ananievskaia, L. Nordstierna, M. Ostman, H. Blanck, *Colloid Polym. Sci.* **2019**, *297*, 307–313.
[72] S. R. Abulateefeh, M. Y. Alkawareek, A. M. Alkilany, *Int. J. Pharm.* **2019**, *558*, 291–298.
[73] F. Ahangaran, M. Hayaty, A. H. Navarchian, *Appl. Surf. Sci.* **2017**, *399*, 721–731.
[74] G. Z. Yang, D. Wibowo, J. H. Yun, L. Z. Wang, A. P. J. Middelberg, C. X. Zhao, *Langmuir* **2017**, *33*, 5777–5785.
[75] X. L. Yang, X. J. Ju, X. T. Mu, W. Wang, R. Xie, Z. Liu, L. Y. Chu, *ACS Appl. Mater. Interfaces* **2016**, *8*, 10524–10534.
[76] R. Atkin, P. Davies, J. Hardy, B. Vincent, *Macromolecules* **2004**, *37*, 7979–7985.
[77] L. Gonzalez, M. Kostrzewska, B. G. Ma, L. Li, J. H. Hansen, S. Hvilsted, A. L. Skov, *Macromol. Mater. Eng.* **2014**, *299*, 1259–1267.
[78] M. A. Trojer, A. Ananievskaia, A. A. Gabul-Zada, L. Nordstierna, H. Blanck, *Colloid Interfac Sci* **2018**, *25*, 36–40.
[79] Z. Sun, C. Yang, M. Eggersdorfer, J. Cui, Y. Li, M. Hai, D. Chen, D. A. Weitz, *Chinetsu* **2020**, *31*, 249–252.
[80] L. L. Kong, E. Amstad, M. T. Hai, X. Y. Ke, D. Chen, C. X. Zhao, D. A. Weitz, *Chinetsu* **2017**, *28*, 1897–1900.
[81] Z. Sun, C. Yang, F. Wang, B. Wu, B. Shao, Z. Li, D. Chen, Z. Yang, K. Liu, *Angew. Chem. Int. Ed.* **2020**, *59*, 9365–9369.

[82] S.-S. Liu, C.-F. Wang, X.-Q. Wang, J. Zhang, Y. Tian, S.-N. Yin, S. Chen, *J. Mater. Chem. C* **2014**, *2*, 9431–9438.
[83] C. Wei, Y. X. Du, Y. Y. Liu, X. Q. Lin, C. Zhang, J. N. Yao, Y. S. Zhao, *J. Am. Chem. Soc.* **2019**, *141*, 5116–5120.
[84] W. Li, H. Dong, G. Tang, T. Ma, X. Cao, *RSC Adv.* **2015**, *5*, 23181–23188.
[85] F. X. Liang, B. Liu, Z. Cao, Z. Z. Yang, *Langmuir* **2018**, *34*, 4123–4131.
[86] C. Kaewsaneha, P. Tangboriboonrat, D. Polpanich, M. Eissa, A. Elaissari, *ACS Appl. Mater. Interfaces* **2013**, *5*, 1857–1869.
[87] G. Agrawal, R. Agrawal, *ACS Appl. Mater. Interfaces* **2019**, *2*, 1738–1757.
[88] A. Walther, A. H. E. Muller, *Chem. Rev.* **2013**, *113*, 5194–5261.
[89] A. Kirillova, C. Marschelke, A. Synytska, *ACS Appl. Mater. Interfaces* **2019**, *11*, 9643–9671.
[90] K. H. Ku, Y. J. Lee, G. R. Yi, S. G. Jang, B. V. K. J. Schmidt, K. Liao, D. Klinger, C. J. Hawker, B. J. Kim, *Macromolecules* **2017**, *50*, 9276–9285.
[91] Y. Lan, J. Choi, H. Y. Li, Y. K. Jia, R. J. Huang, K. J. Stebe, D. Lee, *Ind. Eng. Chem. Res.* **2019**, *58*, 20961–20968.
[92] D. Wei, L. L. Ge, S. H. Lu, J. J. Li, R. Guo, *Langmuir* **2017**, *33*, 5819–5828.
[93] S. S. Liu, C. F. Wang, X. Q. Wang, J. Zhang, Y. Tian, S. N. Yin, S. Chen, *J. Mater. Chem. C* **2014**, *2*, 9431–9438.
[94] N. G. Min, T. M. Choi, S. H. Kim, *Macromol. Chem. Phys.* **2017**, *218(2)*, 1600265.
[95] S. N. Yin, C. F. Wang, Z. Y. Yu, J. Wang, S. S. Liu, S. Chen, *Adv. Mater.* **2011**, *23*, 2915–++.
[96] G. S. Song, M. Chen, Y. R. Zhang, L. Y. Cui, H. B. Qu, X. C. Zheng, M. Wintermark, Z. Liu, J. H. Rao, *Nano Lett.* **2018**, *18*, 182–189.
[97] Y. L. Fan, C. H. Tan, Y. S. Lui, D. Zudhistira, S. C. J. Loo, *RSC Adv.* **2018**, *8*, 16032–16042.
[98] N. G. Min, M. Ku, J. Yang, S. H. Kim, *Chem. Mater.* **2016**, *28*, 1430–1438.
[99] H. Xie, Z. G. She, S. Wang, G. Sharma, J. W. Smith, *Langmuir* **2012**, *28*, 4459–4463.
[100] E. Dehghani, M. Salami-Kalajahi, H. Roghani-Mamaqani, *Colloids Surf. B* **2018**, *170*, 85–91.
[101] O. B. Garbuzenko, J. Winkler, M. S. Tomassone, T. Minko, *Langmuir* **2014**, *30*, 12941–12949.

Manuscript received: June 28, 2020
Revised manuscript received: August 2, 2020
Accepted manuscript online: August 7, 2020

MINIREVIEWS

Mixing matters: Co-precipitation under rapid mixing and controlled phase separation by tuning the interfacial tensions are versatile method to prepare occluded particles, core-shell capsules, dimer particles and heteroaggregates. This Minireview outlines the formation and applications of these particles, which provide countless interesting possibilities in functional materials, colloidal surfactants, imaging, cargo encapsulation and drug delivery.